Inflammation Research
https://doi.org/10.1007/s00011-024-01944-y

ORIGINAL RESEARCH PAPER

The protective role of RACK1 in hepatic ischemia–reperfusion injury-induced ferroptosis

Zelong Yang[1] · Wenjie Gao[1] · Kai Yang[1] · Weigang Chen[1] · Yong Chen[1]

Received: 6 February 2024 / Revised: 28 August 2024 / Accepted: 30 August 2024

Abstract

Although ferroptosis plays a crucial role in hepatic ischemia–reperfusion injury (IRI), the molecular mechanisms underlying this process remain unclear. We aimed to explore the potential involvement of the receptor for activated C kinase 1 (RACK1) in hepatic IRI-triggered ferroptosis. Using hepatocyte-specific RACK1 knockout mice and alpha mouse liver 12 (AML12) cells, we conducted a series of in vivo and in vitro experiments. We found that RACK1 has a protective effect on hepatic IRI-induced ferroptosis. Specifically, RACK1 was found to interact with AMPKα through its 1–93 amino acid (aa) region, which facilitates the phosphorylation of AMPKα at threonine 172 (Thr172), ultimately exerting an antiferroptotic effect. Furthermore, the long noncoding RNA (lncRNA) ZNFX1 Antisense 1 (ZFAS1) directly binds to aa 181–317 of RACK1. ZFAS1 has a dual impact on RACK1 by promoting its ubiquitin–proteasome-mediated degradation and inhibiting its expression at the transcriptional level, which indirectly exacerbates hepatic IRI-induced ferroptosis. These findings underscore the protective role of RACK1 in hepatic IRI-induced ferroptosis and showcase its potential as a prophylactic target for hepatic IRI mitigation.

Keywords RACK1 · Hepatic ischemia–reperfusion injury · Ferroptosis · AMPKα · ZFAS1

Introduction

Hepatic IRI, a leading cause of liver damage during surgeries such as resection, transplantation, trauma, and hypovolemic shock, remains a significant challenge despite medical and surgical advancements [1]. In liver transplantation, hepatic IRI is a complex injury that increases the rate of graft rejection by more than 10% [2]. Due to the shortage of donor livers, marginal grafts are used, which further increases the incidence of hepatic IRI and its complications [3]. The mechanisms underlying hepatic IRI include inflammation, oxidative damage, mitochondrial dysfunction, reactive oxygen species (ROS) production, Kupffer cell activation, apoptosis, and proinflammatory cytokine production [4]. However, no approved and effective strategy for hepatic IRI prevention exists, emphasizing the need for further mechanistic studies with clinical translational importance [5]. Recent research has demonstrated that ferroptosis inhibitors, such as ferrostatin-1 (Fer-1) and liproxstatin-1, have shown efficacy in protecting against cell death in animal ischemia/reperfusion models [6, 7]. Alleviating ferroptosis may represent an effective therapeutic strategy for the treatment of hepatic IRI, yet there is currently a lack of targeted molecular interventions.

RACK1 is a well-established scaffold protein for multiple kinases and receptors due to its structural characteristic of having a seven-bladed β-propeller configuration, which is typical of other WD domain proteins [8, 9]. Previous research has reported the multitudinous roles of RACK1 in organ ischemia–reperfusion injury. For example, the loss of RACK1 was found to protect rats from stroke brain injury [10], whereas the high RACK1 expression caused by ER stress preconditioning could protect the myocardium of diabetic rats from ischemia–reperfusion injury [11]. However, whether RACK1 can participate in hepatic IRI by regulating

Zelong Yang, Wenjie Gao and Kai Yang contributed equally to this work and share the first authorship.

Communicated by John Di Battista

✉ Yong Chen
gdwkcy@163.com

[1] Department of Hepatobiliary Surgery, Xi Jing Hospital, Air Force Medical University, Xi'an 710032, China

Published online: 18 September 2024

ferroptosis is still unclear, and its related mechanisms are unknown.

Our research group has long focused on the pathophysiological role of RACK1. To investigate whether RACK1 is associated with ferroptosis in hepatocytes induced by hepatic IRI, we utilized a mouse model with hepatocyte-specific knockout of the RACK1 gene and conducted a series of experiments to preliminarily demonstrate that RACK1 plays a protective role in hepatic IRI-induced ferroptosis and elucidate the underlying molecular mechanisms involved.

Methods

Mice

The animal experiments were conducted with the approval of the Committee on Animal Care and Use of the Airforce Military Medical University. This study utilized RACK-$1^{flox/flox;\ Alb-Cre}$ mice (8 weeks old) on a C57BL/6J background, which were generated via the Cre-LoxP system at the Shanghai Model Organisms Center, Inc. Tamoxifen was administered through intraperitoneal injection to initiate Cre recombinase activity. Homozygous mice were obtained and crossed with hepatocyte-specific Cre recombinase-expressing mice. $RACK1^{flox/-;\ Alb-Cre}$ mice were used as controls throughout the study, and the mice were divided into different groups based on treatment.

Table 1 The sequences of the siRNAs of RACKI, VDAC2 and siZ-FAS1

siRNA	Sequence (5'-3 ')
siRACK1-1 S	GCUAAAGACCAACCACAUUTT
siRACK1-1 A	AAUGUGGUUGGUCUUUAGCTT
siRACK1-2 S	GCAAGCACCUCUACACUUUTT
siRACK1-2 A	AAAGUGUAGAGGUGCUUGCTT
siRACK1-3 S	GGUCCAGGAUGAGAGUCAUTT
siRACK1-3 A	AUGACUCUCAUCCUGGACCTT
siVDAC2-1 S	GAGGCUUAAUCCAGUUAAATT
siVDAC2-1 A	UUUAACUGGAUUAAGCCUCTT
siVDAC2-1 S	GCUACACACAAAUGUAAAUTT
siVDAC2-2 A	AUUUACAUUUGUGUGUAGCTT
siVDAC2-3 S	GUCAACAACUCUAGUUUAATT
siVDAC2-3 A	UUAAACUAGAGUUGUUGACTT
siZFAS1-1 S	GCCAAGGUCUAUAUAAGGATT
siZFAS1-1 A	UCCUUAUAUAGACCUUGGCTT
siZFAS1-2 S	CAUGUGCACUAUUGCUGGATT
siZFAS1-2 A	UCCAGCAAUAGUGCACAUGTT

S: Sense. A: Anti-Sense

Culturing of cells and treatment in vitro

AML12 cells were cultured in DMEM supplemented with 10% defined FBS, insulin (1 mg/mL), transferrin (0.55 mg/mL), and sodium selenite (0.5 µg/mL) (ITS, cat. no. I3146, Sigma–Aldrich, USA), as well as dexamethasone (40 ng/mL) (cat. no. D8040, Solarbio, China). Transfection with the plasmid vector pcDNA3.1 was performed using Lipofectamine™ 3000 (cat. no. L3000001, Invitrogen, USA), and siRNAs targeting RACK1 (siRACK1) and VDAC2 (siVDAC2) were obtained from GenePharma Co., Ltd. (Shanghai, China). The medium was supplemented with erastin (10 µmol, cat. no. S7242, Selleckchem, USA) and Fer-1 (1 µmol, cat. no. S7243, Selleckchem) for 48 h after transfection. Erastin was added 4 h before simulated hepatic IRI treatment in vitro, and Fer-1 was added 24 h before hepatic IRI treatment. Hypoxia treatment (5% CO_2, 1% O_2, 94% N_2; 37 °C) was applied for 6 h to simulate ischemia in vitro, after which the cells were cultured under normal conditions for 12 h to simulate reperfusion. The control cells were cultured under normal conditions. The concentrations of erastin and Fer1 used in the study were consistent with those in the published literature [12, 13]. The sequences of the siRNAs used (siRACK1, siVDAC2, and siZFAS1) are detailed in Table 1.

Primary mouse hepatocyte (PMH) culture and treatment

PMHs were obtained from the gene-edited mice through a two-step Percoll gradient method utilizing Hank's buffered salt solution without Ca^{2+} and Mg^{2+} ions (cat. no. 14170112, Gibco) and collagenase buffer containing collagenase (0.5 mg/mL, cat. no. 9001-12-1, Sigma–Aldrich). The isolated PMHs were cleansed with PBS and cultured under the same conditions as the AML12 cells. To promote PMH survival, we supplemented the medium with recombinant mouse hepatocyte growth factor (0.5 µg/mL; cat. no. CC13, Novoprotein Scientific, China). Our in vitro simulated ischemia–reperfusion procedure followed the same conditions as those used for AML12 cells, with predetermined time windows based on preliminary experiments. GenePharma Co., Ltd., provided the ZFAS1 siRNA and lentivirus overexpressing RACK1 (RACK1-LV) for transfection following the manufacturer's protocol. PMHs were treated with erastin and Fer-1 using the same method used for the treatment of AML12 cells.

Mouse hepatic IRI model

Pilot experiments were conducted to determine the reperfusion duration of warm hepatic ischemia–reperfusion injury

in mice. Fer-1 (10 mg/kg) or vehicle was administered intraperitoneally 1 h prior to ischemic treatment. Ischemia was induced by blocking the blood supply from the left and middle lobes of the liver for 60 min, beginning at the onset of ischemia. Reperfusion was restored for 6 h, beginning with the resolution of ischemia on the liver surface. Blood and ischemic lobe samples were then collected. The sham surgery group served as the control group. The Fer-1 dose used in the mice was selected based on published literature [14].

RNA extraction and real-time quantitative PCR (qPCR)

RNA was extracted from cells or liver tissues with TRIzol™ LS reagent (cat. no. 10296028, Invitrogen), which was supplemented with Ambion™ DNase I (cat. no. AM2222, Invitrogen) to prevent DNA contamination. The samples were subjected to reverse transcription and PCR amplification using EXPRESS qPCR Supermix kits (cat. no. 11785200, Invitrogen). Gene expression levels were normalized with β-actin as the internal control, and the primer information is listed in Table 2.

Immunoblotting

Proteins were extracted using RIPA lysis buffer (HY-K1001, Med-Chem Express, USA) containing 1× phosphatase inhibitor cocktails I (HY-K0021) and III (HY-K0023) as well as a protease inhibitor cocktail (HY-K0010, Med-Chem Express). Primary antibodies against RACK1 (1:5000, 66940-1-Ig, Proteintech, USA), SLC7A11 (1:2000, 26864-1-AP, Proteintech), TP53 (1:1000, 2524T, CST, USA), GPX4 (1:5000, ab125066, Abcam, UK), CD71 (1:500, WL03500, Wanleibio), FTH1 (1:1000, A19544, ABclonal, China), COX2 (1:1000, WL01750, Wanleibio), VDAC2 (1:5000, 11663-1-AP, Proteintech), phospho-AMPKα (Thr172, p-AMPKα; 1:1000, AF3423, Affinity, China), AMPKα (1:1000, WL02254, Wanleibio), GAPDH (1:1000, WL01114, Wanleibio), and β-actin (1:400, WL01372, Wanleibio) were used, followed by HRP-conjugated secondary antibodies (goat anti-mouse IgG H&L, 1:5000, WLA024, Wanleibio); goat anti-rabbit IgG H&L, 1:10,000, ab6721, Abcam). Target protein visualization was performed using an enhanced chemiluminescence kit (WLA003, Wanleibio).

Table 2 Sequences of primers used for amplification of target genes

Gene	Primer sequence (5'-3')
Rack1 F	CAAGAAGTTATCAGCACCAG
Rack1 R	CCAATAGTTACCTGCCATAC
ß-actin F	CTGTGCCCATCTACGAGGGCTAT
ß-actin R	TTTGATGTCACGCACGATTTCC
IL-18 F	GGCTGCCATGTCAGAAGA
IL-18 R	CCGTATTACTGCGGTTGT
IL-IO F	TTAAGGGTTACTTGGGTTGC
IL-IO R	GAGGGTCTTCAGCTTCTCAC
Beclinl F	GCTGGAGTTGGATGACG
Beclinl R	GATTGTGCCAAACTGTCC
GPX4 F	CAACCAGTTTGGGAGGC
GPX4 R	CTTGGGCTGGACTTTCAT
FTHI F	TTTGACCGAGATGATGTG
ETH 1 R	TCAGTAGCCAGTTTGTGC
CCL3 F	CTGCCCTTGCTGTTCTTC
CCL3 R	AGTTCCAGGTCAGTGATGTA
ICAMI F	ACCATCACCGTGTATTCGT
ICAMI R	GCTGGCGGCTCAGTATCT
*HlF1α*F	GGTATTATTCAGCACGAC
*HlF1α*R	GAGGGAAACATTACATCA
ZFASI F	AGAGCGTTTGCTTTGTTC
ZFASI R	CTCGCCTCAGGAGTTCA

F: Forward. R: Reverse

Cell viability assay

Cell viability was assessed using a CCK-8 kit (cat. no. CK04, Dojindo, Japan) according to the manufacturer's instructions. After treatment, the cells were cultured in 96-well plates and incubated at 37 °C with 10 μL of CCK-8 solution for 2 h. The absorbance at 450 nm was determined with a microplate reader (800TS, Biotek, USA).

MDA, GSH, GSSG, ferrous iron, and mitochondrial membrane potential measurements

MDA, GSH, and GSSG levels were measured using commercially available kits (WLA048, Wanleibio; BC1170 and BC1180, Solarbio). Ferrous iron levels were assessed using a kit from Abcam (ab83366). The absorbance was measured at 593 nm with a microplate reader. The mitochondrial membrane potential was evaluated using a JC-1 assay kit from Beyotime (C2006) and analyzed by flow cytometry.

ROS and lipid hydroperoxide detection

ROS levels were measured using an ROS Assay Kit (WLA131, Wanleibio). The cells were washed twice with PBS and treated with DCFH-DA diluent (diluted 1:1000 in medium) for 30 min in the dark. The fluorescence intensity was analyzed via a flow cytometer (NovoCyte, Agilent, USA). Lipid hydroperoxide levels were determined with a C11 BODIPY 581/591 Assay Kit (D3861, Invitrogen) following the manufacturer's protocol. Flow cytometric data were analyzed with NovoExpress (version 1.4.1). Fresh tissues were sliced and incubated with dihydroethidium (D7008, Sigma–Aldrich) for 30 min. Images were taken with a fluorescence microscope (Nikon Eclipse C1, Nikon, Japan).

Transmission electron microscopy (TEM)

The samples were fixed in a buffered solution containing 2.5% glutaraldehyde (cat. no. G7776, Sigma–Aldrich) and 4% paraformaldehyde. After washing with sucrose–phosphate buffer, the specimens were postfixed with OsO4, and thin 50 nm sections were obtained. The samples were then subjected to TEM (JEM-1400PLUS, JEOL, Japan) and stained using a double-contrast method for examination.

Glycogen periodic acid–Schiff (PAS) and immunofluorescence staining

Glycogen PAS staining (kit cat. no. G1360, Solarbio) was performed on PMH cells following fixation with 4% paraformaldehyde, washing with PBS, oxidant treatment, staining with Schiff's reagent, and counterstaining with hematoxylin solution. Primary hepatocytes were fixed, blocked and then labeled with high-quality primary antibodies against cytokeratin 18 (1:500, cat. no. ET1603-8, Huabio, China), RACK1 (1:800, cat. no. 66940-1-Ig, Proteintech), and p-AMPKα (1:500, cat. no. AF3423, Affinity), which were visualized using the corresponding highly specific secondary antibodies: Cy3-labeled goat anti-rabbit IgG H&L (1:200, cat. no. A0516, Beyotime) and FITC-labeled goat anti-mouse IgG H&L (1:200, cat. no. A0516, Beyotime).

Liver histology and serum parameters

Liver injury severity was evaluated according to the Suzuki score criteria [15], with higher scores indicating more severe damage. The histological features of the liver tissue sections were observed and assessed using hematoxylin and eosin (H&E) staining. Serum levels of aspartate aminotransferase (AST), aminotransferase (ALT), and lactate dehydrogenase (LDH) were measured using ELISA kits (cat. no. SEA207Mu, SEB214Mu, and SEB864Mu, respectively) from Cloud-Clone, China.

Liquid chromatography-tandem mass spectrometry (LC–MS/MS) analysis

The AML12 cells in the control and treatment groups were submitted to Bioengineering Co., Ltd., for immunoprecipitation and LC–MS/MS analyses. Mass spectrometry data were collected using the Triple TOF 5600 + LC/MS system (AB SCIEX, USA). The original MS/MS files were submitted to ProteinPilot (version 4.5, SCIEX, Redwood City, California, USA) for data analysis. In this way, all proteins that may bind to RACK1 can be collected and used for further research.

Coimmunoprecipitation

To fully lyse the AML12 cells, the lysate was centrifuged at 12,000 rpm for 10 min, and the resulting supernatant was collected. The remaining lysate was incubated overnight at 4 °C with anti-RACK1 (1:50, cat. no. 5432 S, CST) and anti-AMPKα (1:100, cat. no. 2532 S, CST) antibodies. After washing with lysis buffer, Pierce™ Protein A/G agarose beads (cat. no. 88802, Thermo Fisher Scientific) were added and incubated overnight, followed by centrifugation. The beads were washed three times with lysis buffer before adding 2× SDS loading buffer and incubating at 95 °C for 5 min. Immunoblotting analysis was performed using an HRP-conjugated goat anti-rabbit IgG H&L secondary antibody (1:10000, cat. no. ab6721, Abcam).

Glutathione S-transferase (GST) pull-down assay

Equal amounts of GST-tagged fusion protein (GST-RACK1 and GST-RACK1 truncations) and His6-tagged fusion protein (His-AMPKα) were incubated for 3 h, loaded onto glutathione Sepharose 4B resin columns, and washed five times with wash buffer. Elution was performed with reduced glutathione-supplemented wash buffer. The eluates were assessed by SDS–PAGE, transferred to PVDF membranes, and subjected to anti-His (His-Tag monoclonal antibody, 1:1000, cat. no. CSB-MA000159, CUSABIO, USA) antibody probing. The negative controls were GST and His6 from Wuhan Genecreate. A GST monoclonal antibody (1:1000, cat. no. CSB-MA000304, CUSABIO) was used as another primary antibody. HRP-conjugated goat anti-mouse IgG H&L (1:5000, cat. no. WLA024, Wanleibio) served as the secondary antibody. Furthermore, we utilized a GST pulldown assay combined with qPCR to determine the exact structural domains involved in the binding of RACK1 to ZFAS1.

RNA immunoprecipitation (RIP)

The interaction between ZFAS1 and RACK1 was studied using an EZ-Magna RIP™ RNA-Binding Protein Immunoprecipitation Kit (cat. no. 17–701, Sigma-Aldrich). AML12 cells were lysed, and the lysates were incubated with antibodies targeting RACK1 and an isotype control IgG to obtain RNA–protein complexes. The immune complexes were then purified using protein A agarose beads. ZFAS1 quantification was carried out using qPCR with the same aforementioned antibodies.

Statistical analysis

For data analysis and visualization, two powerful tools were used: GraphPad Prism 8.0 (GraphPad Inc., San Diego) and SPSS version 26.0 (IBM Corp., Armonk). The data were evaluated for normality and variance homogeneity using the Shapiro–Wilk normality test and the F test. Statistical analysis included the Kruskal–Wallis nonparametric test with post hoc Bonferroni correction for nonnormally distributed data, ANOVA test and Tukey's post-hoc test for normally distributed data among groups and two-tailed Student's t and nonparametric Mann–Whitney U tests for pairwise comparisons between two groups. The results were considered significant at $p < 0.05$.

Results

RACK1 protects against ferroptosis induced by ischemia reperfusion injury (IRI) in vitro

The efficacies of both RACK1 overexpression and knockdown were established (Figure S1 A–B). We found that transcription levels of genes related to hypoxia-inducible factors, inflammatory cytokines, apoptosis, and ferroptosis were altered by IRI, RACK1 expression, or their combined effect, suggesting RACK1's multifaceted roles in hepatic IRI (Figure S1C). Among various phenotypes, we decided to investigate the role of RACK1 in IRI-induced ferroptosis. We found that cell viability decreased in the IRI group compared to the control group, but was restored to normal levels after treatment with Fer1 (IRI + Fer1). In the cells with RACK1 knockdown undergoing IRI, viability was significantly lower than in the IRI group ($p < 0.001$), but was notably restored after treatment with Fer1 ($p < 0.01$). RACK1 overexpression could rescue the reduced cell viability caused by erastin and also the reduced cell viability caused by IRI + erastin (Fig. 1A–B). The production of lipid ROS is closely related to ferrous ions, so we measured the concentration of Fe^{2+} within the cells. We found that IRI increased the concentration of intracellular Fe^{2+}, while the overexpression of RACK1 and Fer1 each could reduce the IRI-induced increase in ferrous ion concentration. In contrast, siRACK1 exacerbated the IRI-induced Fe^{2+} concentration increase. Notably, neither RACK1 interference nor overexpression alone caused an increase in Fe^{2+} concentration, but the addition of Fer1 after siRACK1 transfection still significantly reduced the Fe^{2+} concentration ($p < 0.05$). This may indicate that Fer1's regulation of Fe^{2+} is independent of RACK1 expression (Fig. 1C, Figure S1D). MDA is a key product of lipid peroxidation. Measuring the MDA levels in cells, we found that RACK1 overexpression reduced the IRI- and erastin-induced MDA increases, while RACK1 interference exacerbated the IRI-induced MDA increase ($p < 0.01$). This exacerbation could be rescued by Fer1. Notably, neither overexpression nor interference of RACK1 significantly impacted MDA production, indicating that RACK1-related ROS changes are insufficient to trigger the Fenton reaction or lipid peroxide accumulation. Thus, RACK1 itself does not significantly affect lipid peroxide accumulation. (Fig. 1D, Figure S1E). Changes in the levels of GSH and GSSG are indirect evidence of lipid peroxide accumulation in ferroptosis. By measuring cellular GSH and GSSG levels, we found that siRACK1 and RACK1-OE alone did not affect these levels. IRI increased GSSG and decreased GSH, indicating enhanced lipid peroxidation. Fer1 and RACK1-OE treatment reversed these IRI-induced changes ($p < 0.05$). siRACK1 further decreased GSH and increased GSSG in IRI-treated cells ($p < 0.05$). RACK1-OE also reversed Erastin-induced GSH and GSSG changes ($p < 0.05$). Thus, RACK1 may mitigate IRI-induced ferroptosis by regulating GSH and GSSG levels (Fig. 1E-F, Figure S1F-G).

We detected typical ferroptosis markers using immunoblotting and found that siRACK1 alone only caused an increase in COX2 protein expression, whereas RACK1-OE alone did not cause an increase in the expression of the markers. This suggests that RACK1 itself has a negligible regulatory effect on the ferroptosis-related pathways in cells without IRI induction. IRI increased the expression of TP53 and COX2, and RACK1 overexpression or interference did not affect TP53 changes but affected COX2 changes. Most importantly, RACK1 overexpression protected GPX4 from the IRI-induced decrease, while siRACK1 exacerbated the reduction of GPX4. Additionally, RACK1 overexpression protected VDAC2 from the IRI-induced decrease, whereas siRACK1 aggravated its reduction. Other markers showed inconsistent expression levels with RACK1 overexpression and interference, suggesting that RACK1 might have a complex regulatory role in ferroptosis. Therefore, through semi-quantitative analysis, we suggested that RACK1 might regulate IRI-induced ferroptosis by modulating GPX4 and COX2-related pathways (Fig. 1G–J).

By measuring intracellular ROS levels, we found that IRI increased ROS accumulation compared to the control group. Overexpressing RACK1 reduced ROS levels, indicating RACK1 plays a role in cellular energy consumption and oxidative respiration even without IRI. In cells overexpressing RACK1, whether subjected to IRI or treated with erastin, ROS accumulation significantly decreased. The ferroptosis inhibitor Fer1 completely restored the IRI-induced ROS increase to normal levels, suggesting that IRI-induced ROS generation is largely mediated by ferroptosis. Knocking down RACK1 increased ROS levels, which could be

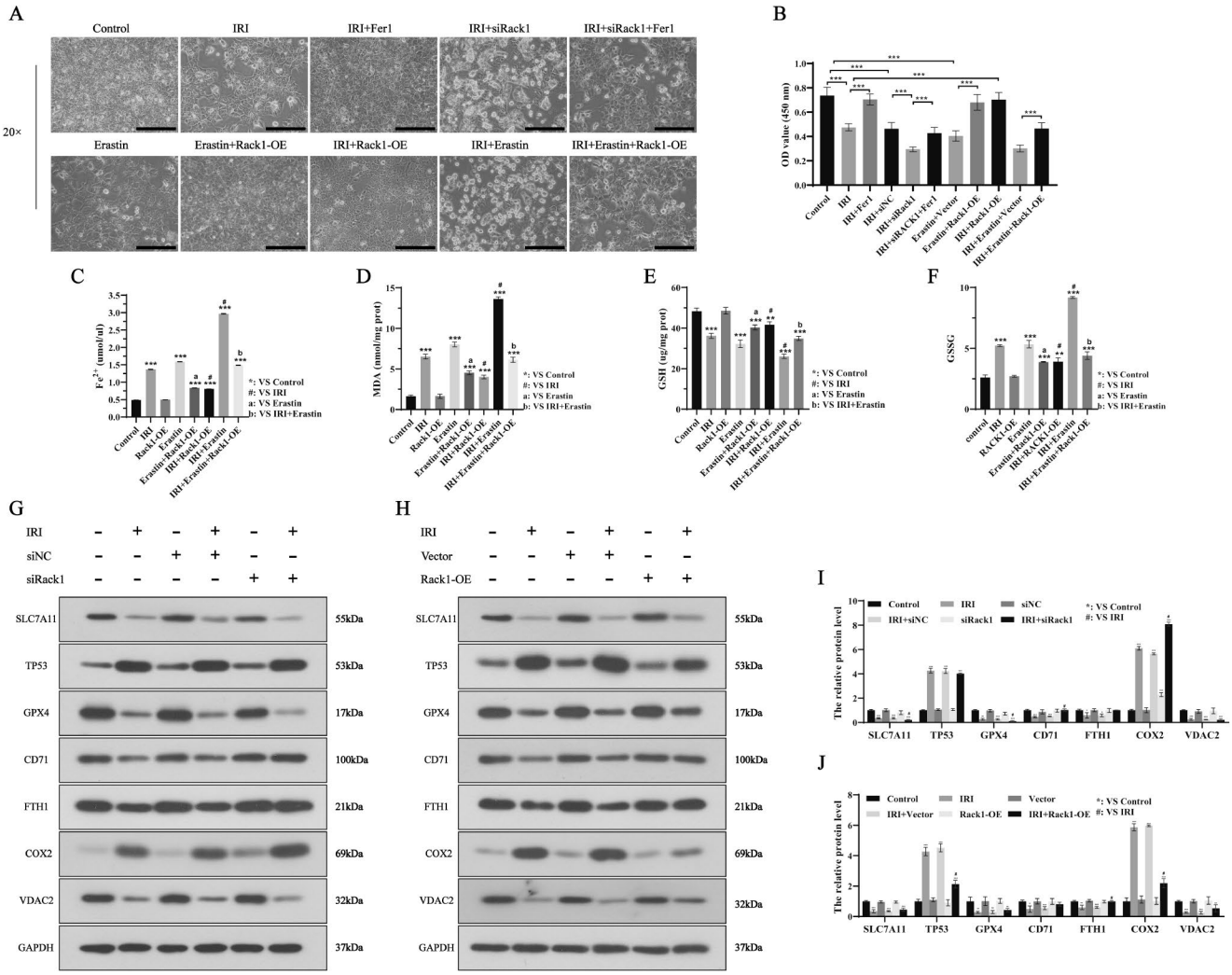

Fig. 1 RACK1 reduces the levels of MDA, ferrous ions, and GSSG induced by simulated IRI while increasing the concentration of reduced GSH. Additionally, RACK1 effectively modulates the expression of ferroptosis biomarkers in AML12 cells. **A-B**: RACK1 alleviated the decrease in cell viability induced by IRI or erastin. **C-F**: RACK1 significantly inhibited MDA, Fe^{2+}, and GSSG levels while decreasing GSH levels in cells after IRI. **G-H**: Immunoblotting of ferroptosis markers in each group. **I-J**: Quantitative analysis of immunoblotting. NC indicates negative control. OD indicates optical density. OE indicates overexpression. The black bar represents 100 μm. $^{*}p < 0.05$, $^{a}p < 0.05$, $^{b}p < 0.05$, $^{\#}p < 0.05$, $^{**}p < 0.01$, $^{***}p < 0.001$

lowered by adding Fer1, corroborating the overexpression results. siRACK1 also exacerbated the IRI-induced ROS increase, which could be rescued by Fer1. Statistical differences were observed between the groups ($p < 0.05$). Therefore, RACK1 could negatively regulate IRI- and erastin-induced ROS accumulation in vitro (Figure S2A–B). One characteristic of ferroptosis is the accumulation of lipid peroxides. We found that IRI indeed increases lipid peroxide levels, while RACK1 overexpression can reduce the IRI-induced increase in lipid peroxides. Conversely, RACK1 knockdown enhances the IRI-induced elevation of lipid peroxides. This enhancement effect can also be inhibited by Fer1 (Fig. 2A). We assessed the mitochondrial membrane potential using JC1. We found that IRI significantly depolarizes the mitochondrial membrane potential, increasing it severalfold. However, in RACK1-overexpressing cells subjected to IRI, the mitochondrial membrane potential exhibited mild depolarization, with no significant difference compared to the control group ($p > 0.05$). Conversely, siRACK1 cells displayed a higher level of depolarization after IRI, which was significantly reduced upon the addition of Fer1 (Fig. 2B). Using transmission electron microscopy, we observed subcellular structures. Mitochondria exhibiting ferroptosis characteristics were marked by red arrows, while normal mitochondria in the control group were marked by green arrows. IRI treatment induced characteristic changes of ferroptosis in mitochondria. The IRI + siRACK1 group exhibited the most numerous mitochondria with pronounced

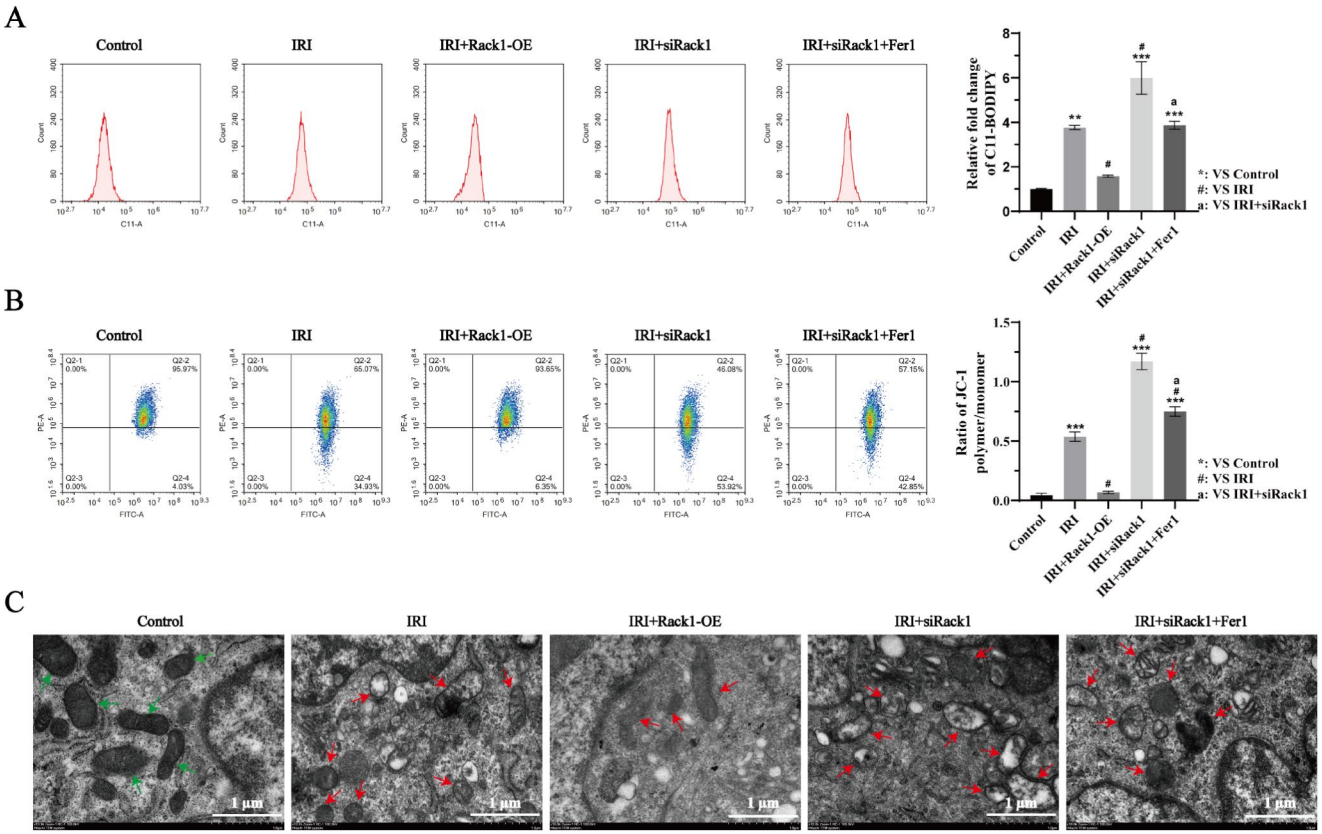

Fig. 2 RACK1 reduces lipid peroxidation, and the mitochondrial membrane potential in AML12 cells after IRI, safeguarding mitochondria from ferroptosis-related alterations. **A**: Detection of lipid peroxide levels in each group. **B**: RACK1 upregulation decreased the increase in the mitochondrial membrane potential induced by IRI, while RACK1 interference significantly exacerbated this change. **C**: Representative TEM images. Green arrows represent normal mitochondria, and red arrows indicate damaged mitochondria. OE indicates overexpression. $^{a}p < 0.05$, $^{\#}p < 0.05$, $^{**}p < 0.01$, $^{***}p < 0.001$

features of ferroptosis, including loss or fragmentation of cristae, mitochondrial swelling, and even rupture with a noticeable reduction in contents. These typical ferroptosis-associated mitochondrial changes were reduced in the IRI + RACK1-OE and IRI + siRACK1 + Fer1 groups. Conversely, cells with enhanced RACK1 expression demonstrated improved mitochondrial integrity (Fig. 2C).

RACK1 protects PMHs from IRI-induced ferroptosis

We employed the Cre-loxp system to specifically knock out RACK1 in mouse hepatocytes. The gene-edited mice were designated RACK1$^{flox/flox;\ Alb-Cre}$ mice and RACK-1$^{flox/-;\ Alb-Cre}$ mice. Figure S3A showed the targeting vector used for this process, which was 16.61 kb in length. The main components of this vector included the MC1-TK-polyA promoter, PGK-Neo-polyA promoter, the flox region, and some resistance genes. The purpose of this plasmid was to replace the original mouse sequence with the exon 3 sequence flanked by flox sequences through homologous recombination. We isolated primary mouse hepatocytes (PMHs) from the gene-edited mice using a two-step method. The cells were cultured under the conditions specified for AML12 cells, with the addition of hepatocyte growth factor to maintain the growth advantage of hepatocytes and to further eliminate the interference of non-parenchymal cells. To validate the efficiency of the primary hepatocyte isolation method, based on the relatively specific characteristics of hepatocytes, we performed PAS glycogen staining and CK18 immunofluorescence. PAS staining and CK18 immunofluorescence indicated that the majority of the collected cells were parenchymal hepatocytes, successfully excluding the interference of non-parenchymal cells (Figure S3B–C). The knockout efficiency was approximately 75%. Moreover, the lentivirus-mediated overexpression of RACK1 was notably substantial (Figure S3D–E). By subjecting PMHs from the control group (RACK1$^{flox/-;\ Alb-Cre}$ mice) to simulated ischemic conditions in vitro and measuring cell viability using CCK-8 at 0, 6, 8, 12, and 24 h of ischemia, we found that 80% of the PMHs remained viable after 6 h of hypoxia. To ensure sufficient PMHs for experiments post-reperfusion injury, we selected 6 h as the duration of ischemia simulation (Figure S3F). PMHs from RACK1$^{flox/flox;\ Alb-Cre}$ mice exhibited lower viability after experiencing IRI in vitro

compared to PMHs from RACK1$^{flox/-;\ Alb-Cre}$ mice subjected to the same IRI. This reduced viability could be rescued by Fer1. Notably, both overexpression of RACK1 via RACK1-LV and knockdown of RACK1 in RACK1-KO independently led to changes in cell viability, suggesting that the expression level of RACK1 itself significantly impacts PMHs' viability (Fig. 3A). The specific mechanism through which RACK1 influences cell viability remains uncertain. MDA measurements revealed that the expression of RACK1 alone does not impact the MDA levels in PMHs. However, RACK1 overexpression can rescue the increase in MDA induced by Erastin or IRI ($p < 0.05$), while RACK1 knockout has the opposite effect (Fig. 3B). Alterations in RACK1 expression can independently influence the levels of GSH and GSSG. Following IRI, RACK1 overexpression effectively reversed the IRI-induced decrease in GSH levels and increase in GSSG levels. Conversely, RACK1 knockout amplified the IRI-induced changes in GSH and GSSG levels (Fig. 3C-D). Transmission electron microscopy demonstrated that RACK1 deletion in PMHs resulted in

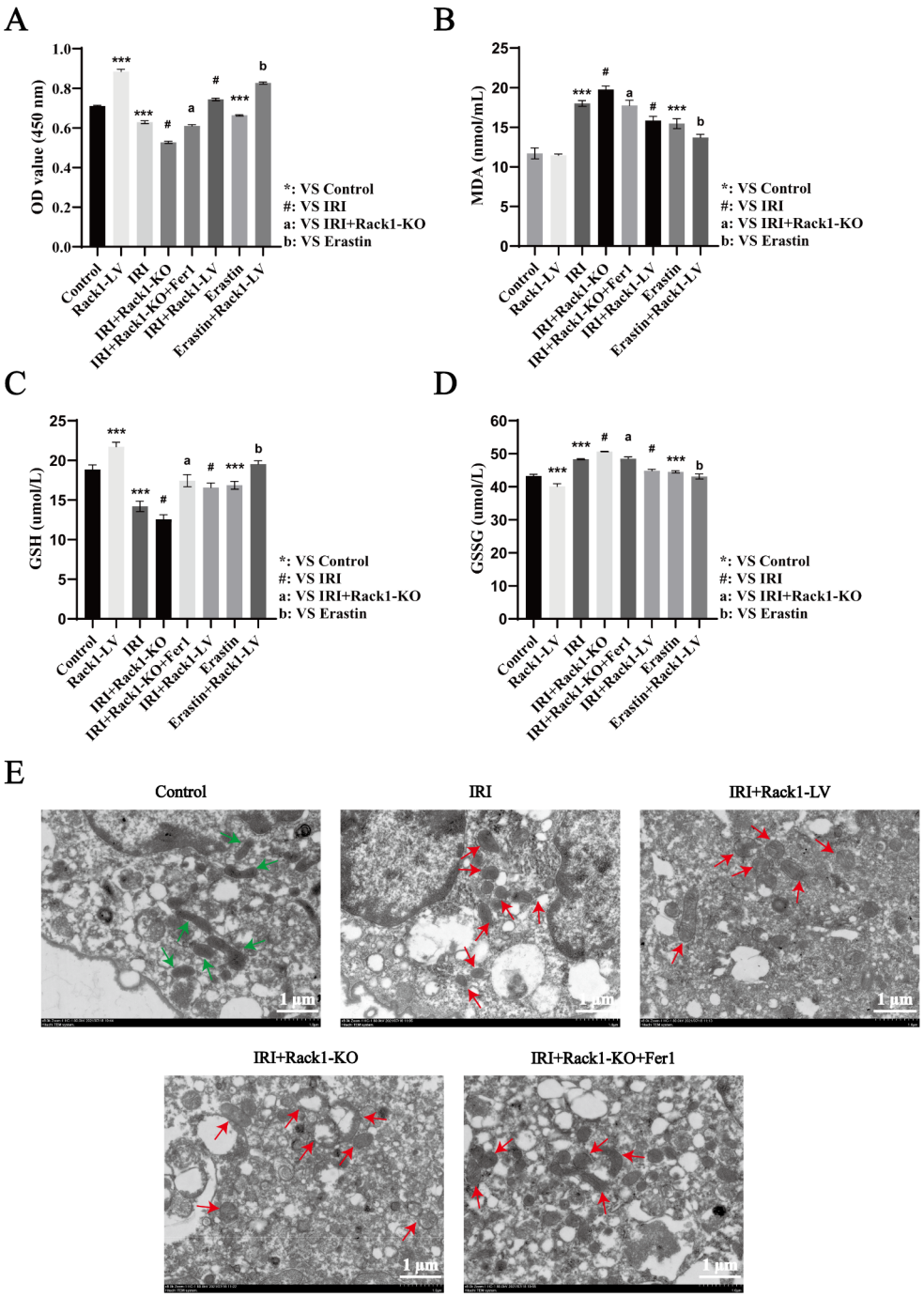

Fig. 3 Knocking out RACK1 leads to intense ferroptosis in PMH cells after IRI. **A**: RACK1-LV improved the reduction in cell viability of PMH cells after IRI, as well as the reduction in cell viability caused by erastin treatment. RACK1-KO further decreased the already reduced viability of PMH cells after IRI, an effect that could be reversed by Fer1. **B**: RACK1-LV reduced the elevated MDA levels in PMH cells after IRI and the elevated MDA levels caused by erastin treatment. RACK1-KO further increased the MDA levels in PMH cells after IRI, an effect that could be partially rescued by Fer1. **C-D**: RACK1-LV reduced the elevated GSSG levels and increased intracellular GSH levels in PMH cells after IRI or erastin treatment. RACK1-KO further increased GSSG levels and decreased GSH levels in PMH cells after IRI, which could be partially rescued by Fer1. **E**: Representative TEM images. Green arrows indicate normal mitochondria; red arrows indicate damaged mitochondria with characteristic changes in ferroptosis. KO indicates knockout. LV indicates lentivirus. $^{a}p < 0.05$, $^{b}p < 0.05$, $^{\#}p < 0.05$, $^{***}p < 0.001$

the most severe mitochondrial impairment following ischemia–reperfusion injury simulation, which was alleviated by Fer-1 administration. Moreover, RACK1 overexpression ameliorated morphological alterations in mitochondria after hepatic IRI treatment (Fig. 3E). By measuring ROS levels in PMHs, we found that Overexpression of RACK1 diminished ROS accumulation induced by IRI, while RACK1 knockout exacerbated it. This exacerbation was mitigated by Fer1 administration (Figure S4A-B). Similarly, examining mitochondrial membrane potential and ferrous ion content in PMHs yielded results consistent with those in AML12 cells. RACK1 overexpression protected against IRI-induced increases in mitochondrial membrane potential and ferrous ion levels, whereas RACK1 knockout worsened these effects and tended to synergize with IRI-induced damage (Fig. 4A-D).

RACK1 knockout exacerbates hepatic IRI-induced liver damage and ferroptosis in vivo

After 1 h of ischemia, blood and liver samples from the mice were collected at each time points during reperfusion (0, 3, 6, 24, and 48 h) for analysis. It was found that the expression of RACK1 and indicators of liver injury exhibited a time-dependent changes following IRI. Both began to rise immediately after ischemia, peaked 6 h after reperfusion, ALT and AST returned to normal by 48 h. The decrease in RACK1 expression was slower, and RACK1 expression remained significantly higher than the control group 48 h after IRI (Figure S5A–C). Based on the above findings, we selected 6 h as the endpoint for reperfusion timing. After grouping the mice according to the predetermined plan and performing the ischemia-reperfusion operation, the levels of ALT, AST, and LDH in the IRI + RACK1-KO group were higher than those in the control group and IRI group, with ALT reaching 181.25 ± 2.65 U/L, AST reaching 180.75 ± 8.63 U/L, and LDH reaching 1315.19 ± 40.46 U/L. However, after treatment with Fer1, these biochemical indicators were significantly reduced, with ALT decreasing to 160.06 ± 8.85 U/L, AST decreasing to 136.64 ± 11.67 U/L, and LDH decreasing to 970.67 ± 118.51 U/L. Significant differences were observed between the groups ($p < 0.05$). (Figure S5D–F).

We used HE staining to assess tissue damage. Compared to the control and IRI groups, the IRI + RACK1-KO group exhibited more severe hepatic tissue damage, characterized by increased cell necrosis, loss of normal hepatic structure, substantial sinusoidal dilation, and more intravascular coagulation. In the IRI + RACK1-KO + Fer1 group, although significant damage was still observed, the severity was improved compared to the IRI + RACK1-KO group. Using the Suzuki scoring system, the IRI + RACK1-KO group had the highest score, with an average of 3.8, while the IRI + RACK1-KO + Fer1 group averaged 2.4 (Fig. 5A). The MDA levels in the liver tissue homogenates of the four groups were measured, revealing that the IRI + RACK1-KO group had the highest MDA level (22.05 ± 1.73 nmol/mg protein). After treatment with Fer1, the MDA level decreased (Fig. 5B). Through TEM, we observed that the mitochondria in hepatocytes of the IRI + RACK1-KO group displayed more pronounced and numerous ferroptosis characteristic changes. These typical ferroptosis-associated mitochondrial alterations were improved in the IRI + RACK1-KO + Fer1 group (Fig. 5C). The GSH and GSSG levels in the tissue homogenates of the four groups were measured. It was found that the IRI + RACK1-KO group had the lowest GSH (17.52 ± 7.78 μmol/L) and the highest GSSG (164.30 ± 12.34 μmol/L). After treatment with Fer1, GSH levels significantly increased (96.32 ± 6.84 μmol/L) and GSSG levels significantly decreased (135.29 ± 2.45 μmol/L) (Fig. 5D-E). Liver tissues were subjected to ROS staining, and the ROS levels were quantified by measuring the mean fluorescence intensity. Compared to the control and IRI groups, the IRI + RACK1-KO group exhibited the highest ROS levels, with a mean intensity of 89.95 ± 7.73 AU. In the IRI + RACK1-KO + Fer1 group, ROS levels significantly decreased, showing a mean intensity of 73.96 ± 2.57 AU (Fig. 5F). NADPH levels were measured, revealing that the IRI + RACK1-KO group had the lowest NADPH content (6.23 ± 2.17 U/g). After treatment with Fer1, NADPH levels significantly increased (16.11 ± 1.80 U/g). There were significant differences between the groups ($p < 0.05$) (Fig. 5G).

RACK1 regulates ferroptosis by directly binding to AMPKα and phosphorylating AMPKα at Thr172

Proteomic profiling via mass spectrometry identified 634 and 646 proteins potentially interacting with RACK1 in the untreated control and IRI groups, respectively, with 381 proteins being common to both groups (Fig. 6A). We performed Gene Ontology (GO) enrichment and Kyoto Encyclopedia of Genes and Genomes (KEGG) analyses of the identified proteins. GO annotations revealed that the majority of proteins interacting with RACK1 were enriched in functions associated with metabolic processes, stress responses, and molecular binding (Figure S6A). According to the KEGG analysis, the identified proteins were enriched in pathways related to amino acid metabolism, lipid metabolism, energy metabolism, cell growth and death, and environmental adaptation (Figure S6B).

In the identified protein profile, we hypothesized that AMPKα might serve as a downstream molecule of RACK1 for several compelling reasons. Firstly, AMPKα acts as a

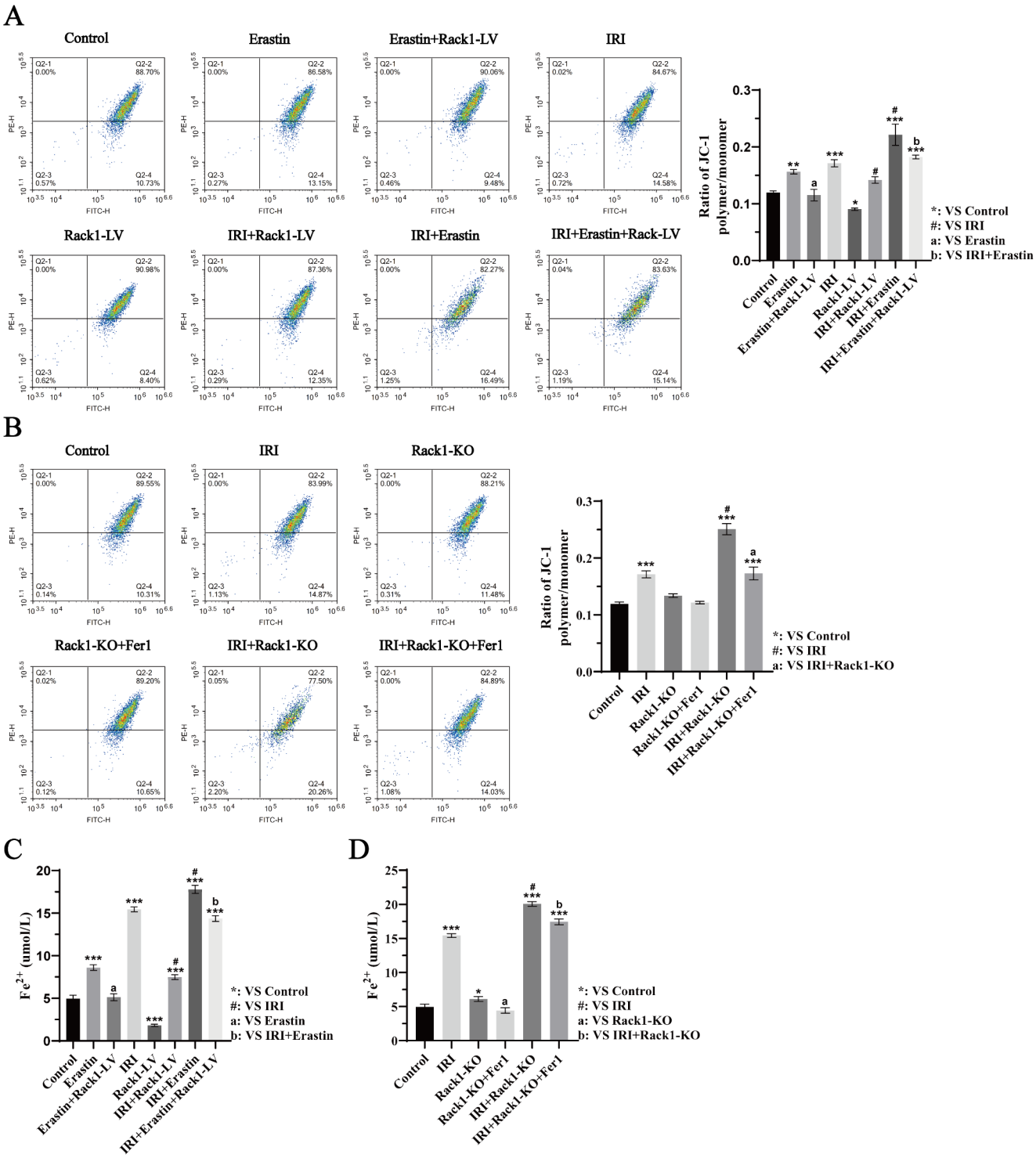

Fig. 4 RACK1 overexpression can inhibit the increase in mitochondrial membrane potential and ferrous ion levels caused by IRI or erastin treatment. Conversely, RACK1 knockout can further promote the increase in mitochondrial membrane potential and ferrous ion levels induced by IRI or erastin treatment, and this further promoting effect can be largely rescued by Fer1. **A–B**: Increasing RACK1 reduced the increase in mitochondrial membrane potential caused by IRI or erastin, while knocking out RACK1 promoted the increase in mitochondrial membrane potential induced by IRI or erastin. **C–D**: Detection of the intracellular ferrous ion concentration in each group. $^{*}p < 0.05$, $^{a}p < 0.05$, $^{b}p < 0.05$, $^{\#}p < 0.05$, $^{**}p < 0.01$, $^{***}p < 0.001$

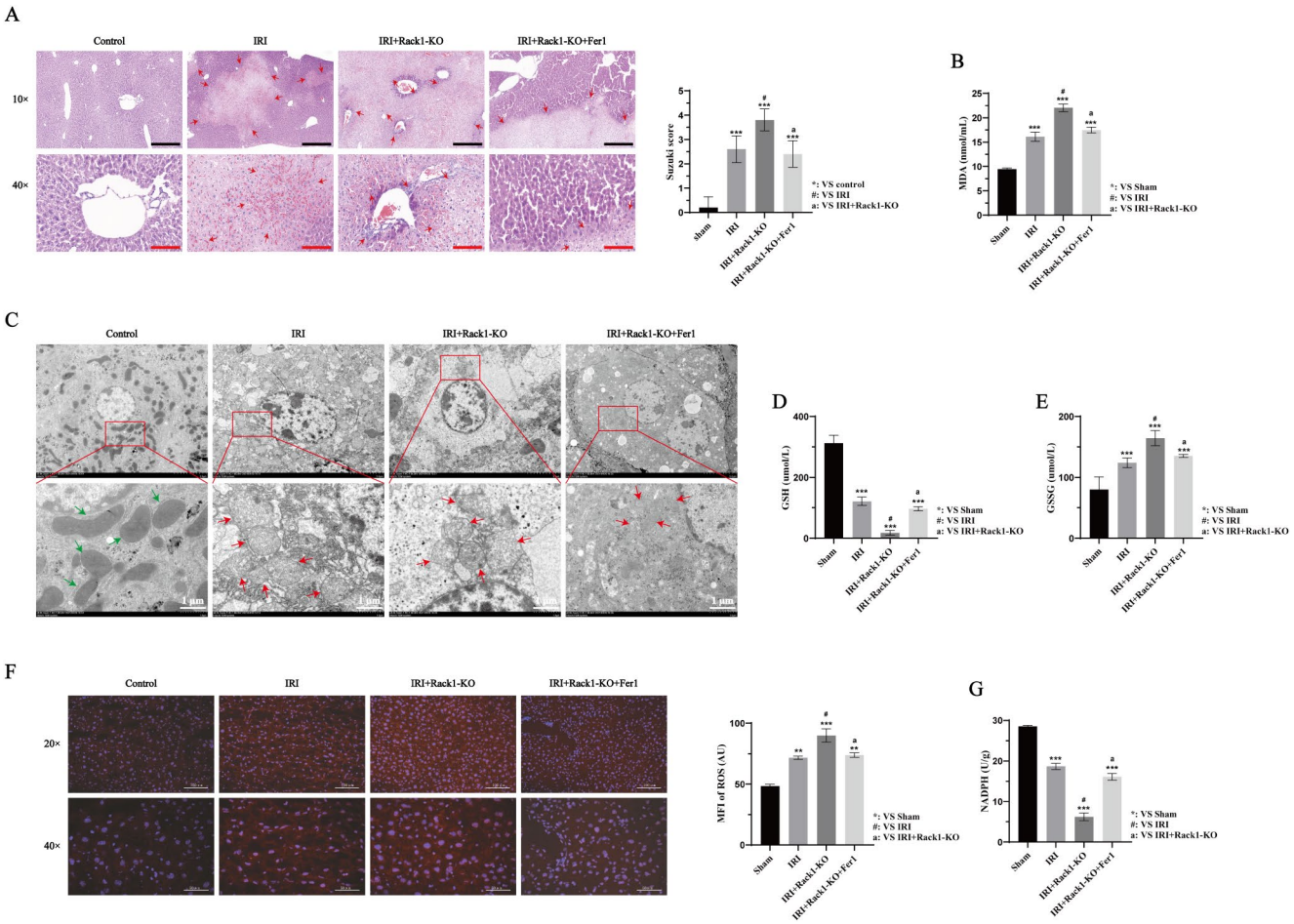

Fig. 5 RACK1 knockout exacerbates liver injury induced by IRI in vivo and increased the level of ferroptosis in liver tissue. **A**: RACK1-KO mice exhibited the most severe liver damage after IRI, which was alleviated after using Fer1. Black bar = 200 μm. Red bar = 50 μm. **B**: RACK1 knockout mice exhibited significantly greater MDA levels following IRI than did control mice; however, these levels were reduced after using Fer1. **C**: Representative TEM images. Green arrows indicate normal mitochondria, and red arrows indicate damaged mitochondria. **D-E**: Compared with heterozygous mice after IRI, RACK1 knockout mice exhibited higher GSSG levels and lower GSH levels. **F**: Fluorescence staining and fluorescence intensity of ROS in each group. MFI indicates mean fluorescence intensity. **G**: RACK1-KO mice had reduced NADPH levels compared to control mice. $^{*}p < 0.05$, $^{a}p < 0.05$, $^{\#}p < 0.05$, $^{**}p < 0.01$, $^{***}p < 0.001$

paramount regulator of cellular energy homeostasis, playing a crucial role in maintaining the balance between energy production and consumption [16]. Secondly, it has been well-documented that AMPKα is integral in modulating oxidative stress responses, a pivotal mechanism underlying ischemia-reperfusion injury. Thirdly, extensive research indicates that AMPKα can induce autophagy, a protective cellular mechanism that mitigates ischemia-reperfusion injury by removing damaged organelles and proteins [17, 18]. Moreover, activation of AMPKα could enhance microvascular endothelial function, thereby facilitating reperfusion and tissue repair in ischemic regions.

We utilized the co-immunoprecipitation to verify protein-protein interactions. In the input group, we detected the target protein signal of RACK1, while no signal was observed in the IgG group. Additionally, the detection of AMPKα protein signal in the input group, but not in the IgG group, suggests that RACK1 can directly bind to AMPKα protein intracellularly (Fig. 6B). We investigated the fluorescence localization of RACK1 and p-AMPKα in AML12 cells under normal conditions and after IRI. We found that after IRI, the fluorescence intensities of both RACK1 and p-AMPKα significantly increased. Moreover, RACK1 and p-AMPKα exhibited colocalization under both normal and IRI conditions (Fig. 6C). Through the GST pulldown assay, we detected AMPKα protein signals in both the RACK1 and RACK1 (1-93aa) groups, indicating that the RACK1 and its (1-93aa) domain can bind to AMPKα. The other two domains (94–180 aa and 181–317 aa) may not directly interact with AMPKα, or their binding abilities to AMPKα may be too weak to detect AMPKα signals (Fig. 6D). Immunoblotting revealed that RACK1 enhances the phosphorylation of AMPKα at threonine 172 , and this effect was markedly amplified following IRI (Fig. 6E- F).

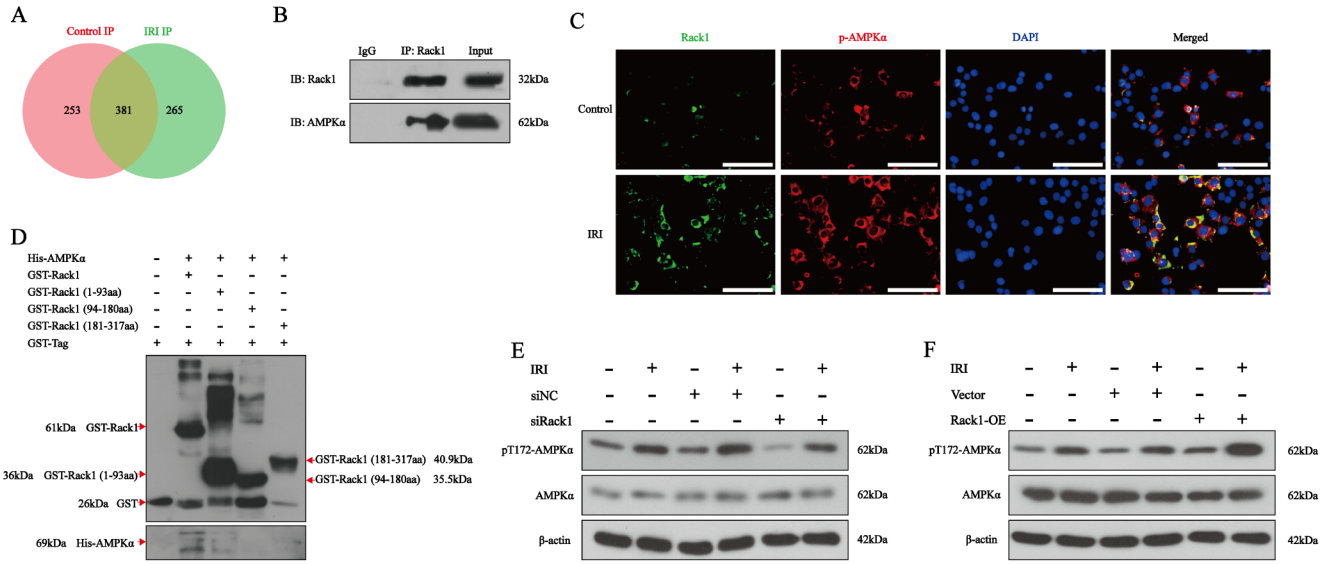

Fig. 6 RACK1 directly interacts with AMPKα and promotes AMPKα phosphorylation at Thr72. **A**: Venn diagram of proteins that may interact with RACK1 under normal conditions and after IRI treatment. **B**: Coimmunoprecipitation confirmed the direct interaction between RACK1 and AMPKα. **C**: RACK1 colocalized with phosphorylated AMPKα in cells. The white bar represents 100 μm. **D**: GST pulldown confirmed that the 1–93 aa of RACK1 binds to AMPKα. **E-F**: Knocking down RACK1 inhibited AMPKα phosphorylation at Thr172, whereas overexpressing RACK1 enhanced its phosphorylation

Due to the potential cytotoxicity of the AMPKα agonist A-769,662, we first determined its optimal working concentration to be 10 μM (Figure S7A-B). In the context of IRI, rescue experiments were conducted by adding the AMPK pathway agonist A-769,662 or the inhibitor Compound C to cells. It was found that overexpression of RACK1 had a protective effect against IRI-induced ROS accumulation, but this protective effect was weakened by Compound C. Conversely, RACK1 knockdown exacerbated IRI-induced ROS accumulation, but this exacerbation was mitigated by A-769,662 (Figure S7C). Likewise, overexpression of RACK1 was shown to reverse ferrous ion accumulation, decreases in cell viability, reductions in GSH, and increases in GSSG in cells subjected to IRI. However, this reversal effect was largely counteracted by the use of Compound C. Conversely, siRACK1 exacerbated the characteristic changes of ferroptosis in cells under IRI conditions, but this exacerbation was ameliorated by the use of A-769,662 (Figure S7D-G). These data indicate that the protective effect of RACK1 is largely mediated through the activation of AMPKα at threonine 172. This conclusion was further confirmed by detecting a series of ferroptosis markers through immunoblotting (Figure S7H).

ZFAS1 aggravates ferroptosis during hepatic IRI by directly binding to RACK1 and downregulating its expression

Recently, the role of ZFAS1 in organ IRI has been increasingly recognized. One study found that ZFAS1 can aggravate myocardial IRI by inducing methylation of the Notch1 gene via DNMT3b recruitment [19]. Conversely, another study showed ZFAS1 alleviates cerebral IRI by regulating miR-421-3p and its target gene MEF2C [20]. However, its role in liver IRI remains unaddressed. Notably, inhibiting ZFAS1 reduces ferroptosis in cells [21], making its role in liver IRI-induced ferroptosis a pertinent question. Using catRAPID (http://service.tartaglialab.com/page/catrapid_omics2_group) [22] and RPISeq (http://pridb.gdcb.iastate.edu/RPISeq/) [23] online tools, we predicted potential interactions between RACK1 and ZFAS1, with probabilities of 64.03% and 96%. Therefore, we chose ZFAS1 as a primary research focus. Additionally, VDAC2, identified through proteomics as a potential interacting molecule with RACK1, was also preselected as a target of our investigation due to its integral role in ferroptosis.

We first validated the effects of both the ZFAS1 overexpression plasmid and siZFAS1 (Fig. 7A-B). Immunoblotting experiments revealed that under normal culture conditions, both ZFAS1 overexpression and VDAC2 interference could disrupt RACK1 expression levels. Comparatively, ZFAS1 overexpression had a more pronounced effect on RACK1. IRI led to an increase in RACK1 expression, which could be reduced by ZFAS1 overexpression but not by VDAC2 interference (Fig. 7C). Consequently, we chose ZFAS1 as the upstream molecule of RACK1 for our subsequent research. At the transcriptional level, we found that ZFAS1 overexpression could reduce RACK1 expression by more than half, while ZFAS1 knockdown could increase RACK1 expression by approximately 2.5-fold ($p < 0.05$) (Fig. 7D).

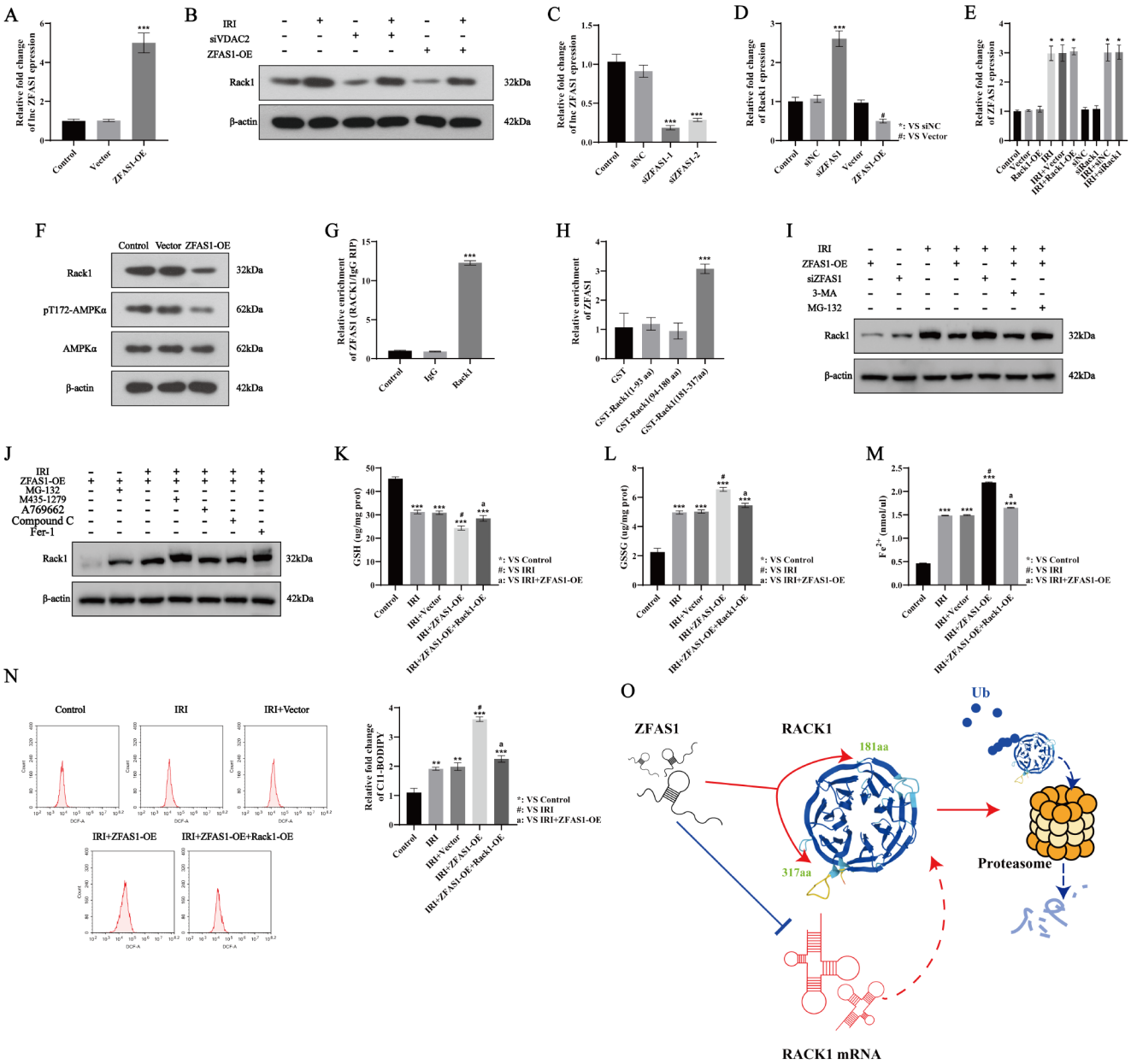

Fig. 7 The upregulation of ZFAS1 inhibits RACK1 transcription and promotes the ubiquitination and degradation of RACK1 protein, thereby exacerbating ferroptosis induced by IRI. **A**: Efficiency validation of ZFAS1 overexpression plasmids. **B**: ZFAS1 upregulation and VDAC2 downregulation significantly inhibited RACK1 expression. **C**: Validation of the efficacy of ZFAS1 siRNAs. **D**: ZFAS1 suppressed the transcriptional expression of RACK1. **E**: Overexpression or knockdown of RACK1 did not affect the transcription level of ZFAS1. **F**: ZFAS1 overexpression reduced AMPKα phosphorylation at Thr172 and suppressed RACK1 protein expression. **G**: RIP assays confirmed the direct interaction between RACK1 and ZFAS1. **H**: The GST pull-down experiment identified that RACK1 interacts directly with ZFAS1 through the domain composed of amino acids 181 to 317. **I-J**: ZFAS1 suppressed the protein levels of RACK1 through the ubiquitin-proteasome pathway. **K–N**: ZFAS1 upregulation worsens the increases in ferrous iron and lipid peroxide levels after IRI, decreases GSH, and increases GSSG. However, RACK1 overexpression reversed these effects. **O**: As shown in the diagram, ZFAS1 suppresses the expression of RACK1 through two mechanisms: first, by inhibiting the transcription of RACK1, and second, by promoting the ubiquitination and degradation of RACK1 protein. OE indicates overexpression. aa indicates amino acids. NC indicates negative control. $*p < 0.05$, $ap < 0.05$, $\#p < 0.05$, $***p < 0.001$

We further discovered that IRI can significantly increase the transcriptional level of ZFAS1. It was also found that under normal conditions or after IRI treatment, neither overexpression nor knockdown of RACK1 could alter the transcriptional level of ZFAS1 (Fig. 7E). The above results indicate that ZFAS1 can inhibit RACK1 expression, whereas RACK1 cannot in turn influence ZFAS1 expression. Therefore, we have clarified that the regulatory direction between

the two is unidirectional, with ZFAS1 unilaterally inhibiting RACK1 expression. Subsequently, we observed that overexpression of ZFAS1 not only reduced the protein expression of RACK1 but also decreased the levels of AMPKα activated at the Thr172 site (Fig. 7F). This suggests that ZFAS1 may influence AMPKα phosphorylation by regulating RACK1 expression, thereby affecting IRI-induced ferroptosis. Using RIP combined with qPCR, we confirmed a direct interaction between RACK1 and ZFAS1 (Fig. 7G), RACK1 binds to ZFAS1 through a domain composed of amino acids 181–317 (Fig. 7H).

Given that ZFAS1 can directly bind to RACK1, we hypothesized that ZFAS1 inhibits RACK1 expression by suppressing its transcription and promoting its degradation post-translationally. Protein degradation in cells typically occurs via either the autophagolysosomal pathway or the ubiquitin-proteasome pathway. To test this, we used 3-MA and MG-132 to inhibit these pathways, respectively. Utilizing a rescue strategy, we conducted immunoblotting to ascertain the specific pathway through which ZFAS1 leads to RACK1 degradation. The results demonstrated that ZFAS1 overexpression indeed inhibits RACK1 protein levels. However, this inhibitory effect was not mitigated by 3-MA treatment, but was significantly reduced by MG-132 treatment. This suggests that ZFAS1 decreases RACK1 expression via the ubiquitin-proteasome pathway (Fig. 7I). M435-1279 is a specific ubiquitination inhibitor of RACK1 [24]. Treatment with MG-132 and M435-1279 can significantly restore RACK1 expression levels in cells with ZFAS1 overexpression, further demonstrating that ZFAS1 promotes the degradation of RACK1 via the ubiquitin-proteasome pathway. When treated with Compound C and A-769,662, the expression levels of RACK1 in ZFAS1-overexpressing cells did not change, which to some extent suggests that the regulation of AMPKα by RACK1 is also unidirectional. Upon addition of Fer1, RACK1 expression was subsequently upregulated, possibly indicating a complex regulatory relationship between RACK1 and ferroptosis (Fig. 7J). In terms of molecular function, the overexpression of ZFAS1 resulted in significant decreases in GSH, increases in GSSG, elevated ferrous ion concentrations, and augmented ROS levels following liver IRI, suggesting that ZFAS1 promotes ferroptosis. The ferroptosis-promoting effect of ZFAS1 can be reversed by the overexpression of RACK1 (Fig. 7K–N). In brief, ZFAS1 inhibits RACK1 expression through both transcriptional and post-translational modifications. The specific mechanisms are illustrated in Fig. 7O.

The ZFAS1/RACK1/AMPKα axis orchestrates ferroptosis induced by IRI

The cell viability in the IRI + siZFAS1 + RACK1-KO group was significantly lower than that in the IRI + siZFAS1 group but higher than that in the IRI + RACK1-KO group. This suggests that inhibiting ZFAS1 expression provides a protective effect against IRI-induced cell death, likely due to an increase in RACK1 expression resulting from the reduction in ZFAS1. Additionally, although the cell viability in the IRI + RACK1-KO group was the lowest, it significantly improved upon the addition of A-769,662. Overexpression of RACK1 exhibits a notable protective effect against IRI-induced declines in cell viability, but this protective effect can be significantly weakened by Compound C (Fig. 8A).

Similarly, the intracellular MDA levels were 18.23 ± 0.89 nmol/mg in the IRI + siZFAS1 + RACK1-KO group, 14.90 ± 0.38 nmol/mg in the IRI + siZFAS1 group, and the highest, 24.65 ± 1.56 nmol/mg, in the IRI + RACK1-KO group. However, after treatment with A-769,662, the intracellular MDA levels in the IRI + RACK1-KO + A769662 group decreased to 18.94 ± 0.76 nmol/mg. Transfection with RACK1-LV significantly reduced the intracellular MDA levels following IRI, decreasing from 19.70 ± 1.46 nmol/mg in the IRI group to 14.39 ± 1.35 nmol/mg in the IRI + RACK1-LV group. However, with the use of Compound C, the MDA levels in the IRI + RACK1-LV + Compound C group were higher compared to the IRI + RACK1-LV group ($p < 0.05$). This indicates that the protective role of RACK1 is mediated by the phosphorylation of AMPKα at Thr172 (Fig. 8B). Reducing ZFAS1, overexpressing RACK1, and activating AMPKα all led to increased intracellular GSH levels and decreased GSSG levels, which is beneficial for cells in resisting IRI-induced ferroptosis. Conversely, reducing RACK1 levels and inhibiting AMPKα activation caused opposite changes in intracellular GSH and GSSG levels, making cells more prone to ferroptosis after IRI treatment (Fig. 8C-D). The results of ROS detection also corroborated this (Fig. 8E). The mechanism diagram of our study results is shown in Fig. 8F.

Discussion

Hepatic IRI, a prevalent and consequential complication following liver surgery or in cases of inadequate tissue perfusion, presents a substantial threat to postoperative recovery. Unfortunately, there are currently no effective treatment options available [25]. Ferroptosis has been shown to play an important role in ischemia-reperfusion injury (IRI) in multiple organs and tissues [26]. The discovery of ferroptosis has significantly changed the academic perspective

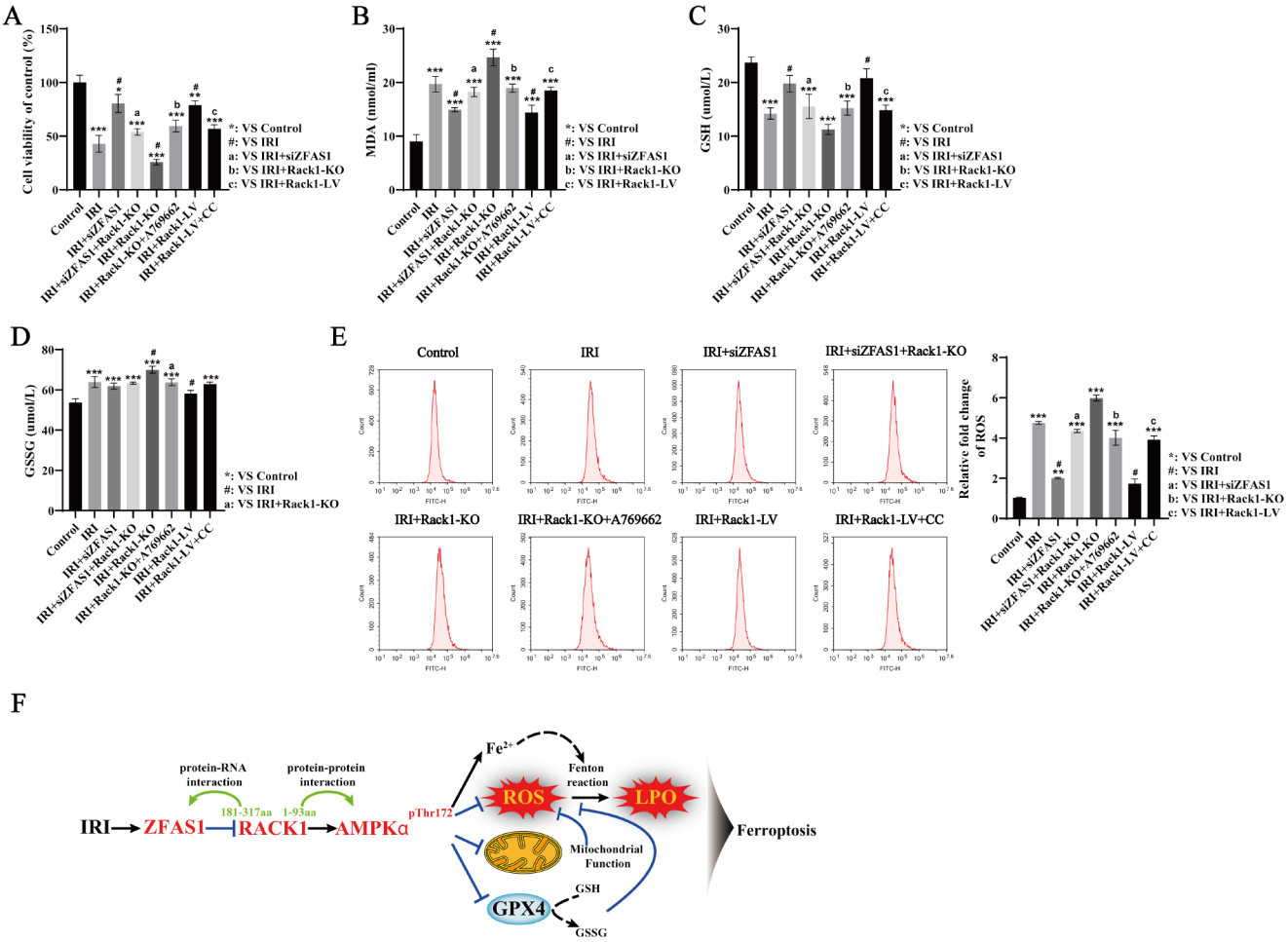

Fig. 8 The ZFAS1/RACK1/AMPKα pathway regulates IRI-induced ferroptosis. **A–E**: Knocking down ZFAS1 improved cell viability after IRI and boosted intracellular GSH levels, while reducing the accumulation of MDA, GSSG, and ROS. However, knocking out RACK1 diminished this protective effect. RACK1 knockout led to elevated ferroptosis levels after IRI, which were alleviated by A769662 treatment. Although RACK1 overexpression safeguarded cells against IRI-induced ferroptosis, Compound C nullified most of this protective benefit. **F**: Diagram of the primary mechanism. LPO indicates lipid peroxidation. CC indicates Compound C. LV indicates lentivirus. $^{a}p < 0.05$, $^{b}p < 0.05$, $^{c}p < 0.05$, $^{\#}p < 0.05$, $^{**}p < 0.01$, $^{***}p < 0.001$

on programmed cell death. Defined by Dixon et al. in 2012 [27], ferroptosis is a novel form of cell death triggered by iron-catalyzed lipid peroxidation. This process leads to lethal levels of lipid peroxides, distinctive mitochondrial changes, unique gene expression patterns, and alterations in metabolic and stress responses.

Liproxstatin-1, a ferroptosis inhibitor that blocks lipid peroxidation independently of GPX4, can alleviate IRI-induced liver damage in mice [28]. Deferoxamine and ferrostatin-1 can inhibit glutamine breakdown and ferroptosis, thereby improving IRI-induced injury in isolated cardiomyocytes [29]. Among the various pathways of cell death implicated in hepatocellular damage associated with IRI, ferroptosis has emerged as a crucial target for therapeutic intervention [30]. However, the mechanisms of ferroptosis in liver IRI are currently insufficiently explored, and further studies are still necessary. Our research provides valuable evidence for the fundamental understanding of this process.

In this study, we successfully constructed hepatocyte-specific RACK1 knockout mice using the Cre-LoxP system, namely $RACK1^{flox/flox;\ Alb\text{-}Cre}$ mice. The control group consisted of $RACK1^{flox/-;\ Alb\text{-}Cre}$ mice. The efficiency of Cre-mediated knockout after tamoxifen induction was approximately 75–80%, which is highly satisfactory considering the presence of other stromal cells and circulating cells in liver tissue. We performed in vivo liver IRI treatment and observed that serum liver injury indicators were significantly higher in RACK1-KO mice compared to heterozygous mice, indicating that IRI causes more severe liver damage in RACK1-KO mice. This indirectly suggests that RACK1 may play a protective role against IRI-induced liver damage. By examining liver tissue homogenates, we found that the levels of MDA and GSSG were higher, while GSH was

lower in the IRI + RACK1-KO group compared to the IRI group. This indicates that RACK1-KO may lead to greater ROS accumulation during IRI, which was confirmed by ROS fluorescence staining of the tissue. At the tissue level, HE staining revealed that RACK1 knockout results in a more extensive area of liver damage following IRI, which is alleviated by the use of a ferroptosis-specific inhibitor. This suggests that RACK1 may play a role in resisting ferroptosis during IRI. TEM revealed characteristic mitochondrial changes of ferroptosis, with varying degrees and quantities observed across different groups. Consistent with histological findings, RACK1 knockout hepatocytes displayed the most numerous and pronounced ferroptosis-associated mitochondrial alterations.

To eliminate the potential influence of mesenchymal and other cell types on liver parenchymal cells, we conducted a series of in vitro experiments using the AML12 cell line and isolated PMHs following IRI treatment. These experiments confirmed that RACK1 has a protective role against ferroptosis. It can inhibit the accumulation of ROS and lipid peroxidation induced by IRI in hepatocytes, reduce the increase in ferrous ion concentration caused by IRI, lower the mitochondrial membrane potential depolarization induced by IRI, and protect the mitochondrial structure from characteristic changes of ferroptosis. Based on immunoblot analysis, we found that RACK1 could protect cells from IRI-induced ferroptosis by preserving GPX4 expression and reducing COX2 expression. It is worth discussing that, in the absence of IRI stimulation, changes in RACK1 expression only resulted in variations in ROS levels, without affecting MDA, mitochondrial membrane potential, iron ion concentration, GSSG, and GSH in AML12 cells. However, in isolated PMHs, changes in RACK1 expression not only altered intracellular ROS levels but also resulted in changes in all these indicators. This discrepancy might be due to the different adaptability of primary hepatocytes and immortalized liver cells to the same culture conditions. It is also possible that a series of changes in gene expression patterns, metabolic patterns, and stress responses occur after the isolation of primary hepatocytes, leading to differences in cellular activity and metabolism between primary hepatocytes and AML12 cells before IRI treatment. Additionally, the methods and vectors used for knocking down or overexpressing RACK1 in the two cell types were also different. These technical differences and variations in cell states may have contributed to the slightly different results.

A study has found that ferroptosis occurs during the reperfusion phase rather than the ischemic phase, as the levels of two key enzymes involved in ferroptosis—GPX4 and long-chain acyl-CoA synthetase 4 (ACSL4)—are significantly regulated only during reperfusion, accompanied by increased iron ion concentration and elevated levels of malondialdehyde [31]. Nevertheless, we found that immediately after IRI, just at the onset of reperfusion, the expression level of RACK1 had already increased severalfold. This indicates that RACK1 may not only play a role during reperfusion but is also upregulated during the ischemic phase via various signaling pathways. This upregulation may be a result of endoplasmic reticulum stress during hypoxia [32].

Using high-throughput immunoprecipitation combined with proteomics, we identified many potential protein interactions with RACK1. We then performed functional and pathway enrichment analyses on these proteins. Many of the enriched pathways and functions are related to energy metabolism. Energy deprivation is an initiating factor for hepatic IRI. During the reperfusion stage, even though blood flow is restored to the liver, hepatocytes remain in an energy-deprived pathological state due to factors like the formation of an inflammatory environment, microvascular emboli, and damage to liver sinusoidal endothelial cells. Therefore, we believe that the protein network identified in this study holds regulatory significance for both stages of hepatic ischemia and reperfusion. Additionally, we identified RACK1-interacting proteins common to both normal and IRI conditions to find molecules that stably bind RACK1 regardless of environmental changes, ensuring the study's consistency. However, we should focus more on proteins that interact with RACK1 in each environment separately, paying particular attention to those that do not interact with RACK1 under normal conditions but do so under IRI conditions. These molecules likely bind to RACK1 due to stress mechanisms, signal transduction, post-translational modifications, or other IRI-induced changes. Research from this perspective may offer new insights into the RACK1-related molecular interaction network in cells experiencing IRI.

The association between the AMPK pathway and ferroptosis has been extensively observed in various diseases. Lee et al. demonstrated that energy stress triggers the activation of the AMPK pathway, leading to the inhibition of ferroptosis and lipid peroxidation [33]. Beclin1 can undergo AMPK activation-dependent phosphorylation, thereby regulating the activity of System Xc− [34]. In the context of myocardial ischemia–reperfusion injury, ferulic acid and Britanin activate the AMPK pathway through distinct mechanisms to alleviate ferroptosis [35, 36]. Our study further corroborates previous research by demonstrating that AMPK activation effectively mitigates ferroptosis in hepatic IRI. It revealed that RACK1 directly interacts with AMPKα and governs the phosphorylation of AMPKα at Thr172 under both normal and hepatic IRI conditions.

Previous research has predominantly concentrated on investigating the causal associations between RACK1 and cellular necrosis, autophagy, and apoptosis subsequent

to organ ischemia–reperfusion injury [37–39]. However, there have been few studies examining the involvement of RACK1 in hepatic IRI-induced ferroptosis. In a preceding investigation, we demonstrated that liver preconditioning can enhance the expression of RACK1, thereby stimulating autophagy in impaired cells, fostering endoplasmic reticulum stress, and impeding cell apoptosis subsequent to hepatic IRI [32]. Through a comprehensive set of functional verification and phenotypic experiments, our study revealed that RACK1 can mitigate ferroptosis during hepatic IRI. Nevertheless, the inhibitory impact of ZFAS1, an upstream molecule, on the protective function of RACK1 is noteworthy, as it hinders the expression of RACK1 and consequently diminishes its protective effects. ZFAS1 can directly interact with the 181–317 amino acid region of RACK1, leading to a reduction in RACK1 expression levels by impeding its transcriptional activity and promoting its degradation through ubiquitin–proteasome-mediated mechanisms.

As previously mentioned, we pre-selected the lncRNA ZFAS1 through literature review and network tool predictions, and validated its role through a series of experiments. Other studies have indirectly supported our hypothesis. ZFAS1 plays a role in and provides protection against ischemic reperfusion injury in the heart and brain, potentially through the regulation of injury-related microRNAs (such as miR-590-3p, miR-582, and miR-761), which are known to enhance anti-apoptotic and antioxidant stress responses [40–42]. ZFAS1 has been identified as a functional long non-coding RNA that binds to protein molecules. For instance, ZFAS1 can bind to the cardioprotective protein SERCA2a, limiting its intracellular levels and inhibiting its activity, thereby exacerbating myocardial infarction damage [43]. As a nucleic acid molecule, ZFAS1 can undergo post-transcriptional modifications. One such modification is its stabilization by the m6A reader molecule IMP2 at the 843rd adenosine. This increased stability allows ZFAS1 to interact with the downstream protein OLA1, altering its conformation and regulating mitochondrial-related energy metabolism in colon cancer cells [44]. Given ZFAS1's strong association with ferroptosis and its functional characteristic of binding proteins, along with our initial hypothesis, we investigated the interaction between ZFAS1 and our target molecule RACK1. Our findings demonstrated that ZFAS1 is an upstream regulator of RACK1, inhibiting its expression at both the transcriptional and post-translational levels. A bioinformatics analysis also indicated that ZFAS1 is involved in protein translation and post-translational ubiquitination [45], which further corroborates our results.

This study has several advantages. First, it employs a high-throughput approach to identify downstream interacting protein molecules of RACK1, which is highly original. Second, it is the first to discover the interaction between RACK1 and ZFAS1. By using inhibitors in combination with rescue strategies, the study determined that ZFAS1 not only inhibits the transcription of RACK1 but also promotes its degradation through the ubiquitin-proteasome system, thereby reducing its levels. These findings have not been previously reported. Third, different rescue strategies confirmed that the ZFAS1/RACK1/AMPKα axis is a unidirectional regulatory pathway for ferroptosis during hepatic IRI.

Nonetheless, it is important to acknowledge the presence of certain limitations. First, although this study identified that the domain composed of 1–93 aa of RACK1 binds to AMPKα and the domain composed of 181–317 aa binds to ZFAS1, it did not specify which particular amino acid residues interact with AMPKα and ZFAS1, indicating a lack of detail in the molecular mechanism. Second, while we demonstrated that RACK1 binds to the aforementioned molecules via specific domains, we did not conduct a reverse study to identify the precise binding interfaces of AMPKα and ZFAS1 with RACK1. Third, although we showed that RACK1 interacts with the two molecules through different domains, we did not ascertain whether the binding interfaces are indispensable for IRI-induced ferroptosis. Specifically, we did not create RACK1 mutants and use rescue strategies to confirm this. Fourth, ferroptosis is a complex form of regulated cell death involving multiple networks. Currently, there is no consensus on the hallmark "executioner" molecules of ferroptosis. Therefore, most of the evidence in this study is indirect, inferred from metabolic products, mitochondrial membrane potential, and other indicators, with direct evidence relying solely on TEM to observe mitochondrial morphology. We believe that with further research on ferroptosis, the characteristic "executioner" molecules will be identified and confirmed.

In summary, RACK1 protects hepatocytes from liver IRI-induced ferroptosis by inhibiting lipid peroxidation, reactive oxygen species accumulation, and the imbalance of the glutathione ratio. RACK1 interacts with AMPKα through its 1–93 amino acid region, promoting the phosphorylation of AMPKα at threonine 172, thereby safeguarding cells against IRI damage. IRI can upregulate the long non-coding RNA ZFAS1, which inhibits RACK1 expression by reducing its mRNA levels. Additionally, ZFAS1 binds to the 181–317 amino acid region of RACK1 and facilitates its degradation via the ubiquitin-proteasome pathway. Hence, the regulation of ferroptosis induced by IRI through the ZFAS1/RACK1/AMPKα axis appears to be unidirectional. RACK1 mitigates ferroptosis by activating AMPKα, whereas ZFAS1 exacerbates ferroptosis by inhibiting RACK1. This newly identified ZFAS1/RACK1/AMPKα axis offers promising new targets and strategies for the treatment and prevention of hepatic IRI, with substantial clinical application potential.

Supplementary Information The online version contains supplementary material available at https://doi.org/10.1007/s00011-024-01944-y.

Author contributions Conceptualization, ZY and YC; methodology, ZY and KY; software, KY and WG; validation, WG and WC; investigation, ZY and KY; resources, ZY; data curation, KY and WC; writing—original draft preparation, ZY; writing—review and editing, ZY and YC; project administration, YC; funding acquisition, YC. All authors have read and agreed to the published version of the manuscript.

Data availability No datasets were generated or analysed during the current study.

Declarations

Competing interests The authors declare no competing interests.

References

1. Ni D, Wei H, Chen W, Bao Q, Rosenkrans ZT, Barnhart TE, et al. Ceria nanoparticles Meet hepatic ischemia-reperfusion Injury: the Perfect Imperfection. Adv Mater. 2019;31(40):e1902956.
2. Du YD, Guo WY, Han CH, Wang Y, Chen XS, Li DW, et al. N6-methyladenosine demethylase FTO impairs hepatic ischemia-reperfusion injury via inhibiting Drp1-mediated mitochondrial fragmentation. Cell Death Dis. 2021;12(5):442.
3. Huang J, Xie P, Dong Y, An W. Inhibition of Drp1 SUMOylation by ALR protects the liver from ischemia-reperfusion injury. Cell Death Differ. 2021;28(4):1174–92.
4. Bavarsad K, Riahi MM, Saadat S, Barreto G, Atkin SL, Sahebkar A. Protective effects of curcumin against ischemia-reperfusion injury in the liver. Pharmacol Res. 2019;141:53–62.
5. Selzner N, Rudiger H, Graf R, Clavien PA. Protective strategies against ischemic injury of the liver. Gastroenterology. 2003;125(3):917–36.
6. Yamada N, Karasawa T, Wakiya T, Sadatomo A, Ito H, Kamata R, et al. Iron overload as a risk factor for hepatic ischemia-reperfusion injury in liver transplantation: potential role of ferroptosis. Am J Transpl. 2020;20(6):1606–18.
7. Li Y, Feng D, Wang Z, Zhao Y, Sun R, Tian D, et al. Ischemia-induced ACSL4 activation contributes to ferroptosis-mediated tissue injury in intestinal ischemia/reperfusion. Cell Death Differ. 2019;26(11):2284–99.
8. Duan F, Wu H, Jia D, Wu W, Ren S, Wang L, et al. O-GlcNAcylation of RACK1 promotes hepatocellular carcinogenesis. J Hepatol. 2018;68(6):1191–202.
9. Adams DR, Ron D, Kiely PA. RACK1, a multifaceted scaffolding protein: structure and function. Cell Commun Signal. 2011;9:22.
10. Li X, Li J, Qian J, Zhang D, Shen H, Li X et al. Loss of ribosomal RACK1 (receptor for activated protein kinase C 1) Induced by Phosphorylation at T50 alleviates cerebral ischemia-reperfusion Injury in rats. Stroke. 2018:STROKEAHA118022404.
11. Yan B, Liu S, Li X, Zhong Y, Tong F, Yang S. Preconditioning with endoplasmic reticulum stress alleviated heart ischemia/reperfusion injury via modulating IRE1/ATF6/RACK1/PERK and PGC-1alpha in diabetes mellitus. Biomed Pharmacother. 2019;118:109407.
12. Wang L, Zhang Z, Li M, Wang F, Jia Y, Zhang F, et al. P53-dependent induction of ferroptosis is required for artemether to alleviate carbon tetrachloride-induced liver fibrosis and hepatic stellate cell activation. IUBMB Life. 2019;71(1):45–56.
13. Sui M, Jiang X, Chen J, Yang H, Zhu Y. Magnesium isoglycyrrhizinate ameliorates liver fibrosis and hepatic stellate cell activation by regulating ferroptosis signaling pathway. Biomed Pharmacother. 2018;106:125–33.
14. Jiang H, Fang Y, Wang Y, Li T, Lin H, Lin J, et al. FGF4 improves hepatocytes ferroptosis in autoimmune hepatitis mice via activation of CISD3. Int Immunopharmacol. 2023;116:109762.
15. Suzuki S, Toledo-Pereyra LH, Rodriguez FJ, Cejalvo D. Neutrophil infiltration as an important factor in liver ischemia and reperfusion injury. Modulating effects of FK506 and cyclosporine. Transplantation. 1993;55(6):1265–72.
16. Herzig S, Shaw RJ. AMPK: guardian of metabolism and mitochondrial homeostasis. Nat Rev Mol Cell Biol. 2018;19(2):121–35.
17. Liu H, Wu X, Luo J, Zhao L, Li X, Guo H, et al. Adiponectin peptide alleviates oxidative stress and NLRP3 inflammasome activation after cerebral ischemia-reperfusion injury by regulating AMPK/GSK-3beta. Exp Neurol. 2020;329:113302.
18. Mohsin AA, Chen Q, Quan N, Rousselle T, Maceyka MW, Samidurai A, et al. Mitochondrial complex I inhibition by metformin limits Reperfusion Injury. J Pharmacol Exp Ther. 2019;369(2):282–90.
19. Li M, Jiao L, Shao Y, Li H, Sun L, Yu Q, et al. LncRNA-ZFAS1 promotes myocardial ischemia-reperfusion Injury through DNA methylation-mediated Notch1 down-regulation in mice. JACC Basic Transl Sci. 2022;7(9):880–95.
20. Xu J, Huang X, Liu S, Chen D, Xie Y, Zhao Z. The protective effects of lncRNA ZFAS1/miR-421-3p/MEF2C axis on cerebral ischemia-reperfusion injury. Cell Cycle. 2022;21(18):1915–31.
21. Ni T, Huang X, Pan S, Lu Z. Inhibition of the long non-coding RNA ZFAS1 attenuates ferroptosis by sponging mir-150-5p and activates CCND2 against diabetic cardiomyopathy. J Cell Mol Med. 2021;25(21):9995–10007.
22. Armaos A, Colantoni A, Proietti G, Rupert J, Tartaglia GG. catRAPID omics v2.0: going deeper and wider in the prediction of protein-RNA interactions. Nucleic Acids Res. 2021;49(W1):W72–9.
23. Muppirala UK, Honavar VG, Dobbs D. Predicting RNA-protein interactions using only sequence information. BMC Bioinformatics. 2011;12:489.
24. Yu Z, Jiang X, Qin L, Deng H, Wang J, Ren W, et al. A novel UBE2T inhibitor suppresses Wnt/beta-catenin signaling hyperactivation and gastric cancer progression by blocking RACK1 ubiquitination. Oncogene. 2021;40(5):1027–42.
25. Liu Y, Lu T, Zhang C, Xu J, Xue Z, Busuttil RW, et al. Activation of YAP attenuates hepatic damage and fibrosis in liver ischemia-reperfusion injury. J Hepatol. 2019;71(4):719–30.
26. Wu Y, Jiao H, Yue Y, He K, Jin Y, Zhang J et al. Ubiquitin ligase E3 HUWE1/MULE targets transferrin receptor for degradation and suppresses ferroptosis in acute liver injury. Cell Death Differ. 2022.
27. Dixon SJ, Lemberg KM, Lamprecht MR, Skouta R, Zaitsev EM, Gleason CE, et al. Ferroptosis: an iron-dependent form of non-apoptotic cell death. Cell. 2012;149(5):1060–72.
28. Friedmann Angeli JP, Schneider M, Proneth B, Tyurina YY, Tyurin VA, Hammond VJ, et al. Inactivation of the ferroptosis regulator Gpx4 triggers acute renal failure in mice. Nat Cell Biol. 2014;16(12):1180–91.
29. Gao M, Monian P, Quadri N, Ramasamy R, Jiang X. Glutaminolysis and transferrin regulate Ferroptosis. Mol Cell. 2015;59(2):298–308.
30. Wu J, Wang Y, Jiang R, Xue R, Yin X, Wu M, et al. Ferroptosis in liver disease: new insights into disease mechanisms. Cell Death Discov. 2021;7(1):276.
31. Tang LJ, Luo XJ, Tu H, Chen H, Xiong XM, Li NS, et al. Ferroptosis occurs in phase of reperfusion but not ischemia in rat heart following ischemia or ischemia/reperfusion. Naunyn Schmiedebergs Arch Pharmacol. 2021;394(2):401–10.

32. Liu D, Liu X, Zhou T, Yao W, Zhao J, Zheng Z, et al. IRE1-RACK1 axis orchestrates ER stress preconditioning-elicited cytoprotection from ischemia/reperfusion injury in liver. J Mol Cell Biol. 2016;8(2):144–56.
33. Lee H, Zandkarimi F, Zhang Y, Meena JK, Kim J, Zhuang L, et al. Energy-stress-mediated AMPK activation inhibits ferroptosis. Nat Cell Biol. 2020;22(2):225–34.
34. Song X, Zhu S, Chen P, Hou W, Wen Q, Liu J, et al. AMPK-Mediated BECN1 phosphorylation promotes ferroptosis by directly blocking System Xc(-) activity. Curr Biol. 2018;28(15):2388–99. e5.
35. Liu X, Qi K, Gong Y, Long X, Zhu S, Lu F et al. Ferulic acid alleviates myocardialischemia reperfusioninjury via upregulating AMPKalpha2 expression-mediated ferroptosis depression. J Cardiovasc Pharmacol. 2021.
36. Lu H, Xiao H, Dai M, Xue Y, Zhao R. Britanin relieves ferroptosis-mediated myocardial ischaemia/reperfusion damage by upregulating GPX4 through activation of AMPK/GSK3beta/Nrf2 signalling. Pharm Biol. 2022;60(1):38–45.
37. Zhao Y, Wang Q, Qiu G, Zhou S, Jing Z, Wang J, et al. RACK1 promotes autophagy by enhancing the Atg14L-Beclin 1-Vps34-Vps15 complex formation upon phosphorylation by AMPK. Cell Rep. 2015;13(7):1407–17.
38. Qian L, Shi J, Zhang C, Lu J, Lu X, Wu K, et al. Downregulation of RACK1 is associated with cardiomyocyte apoptosis after myocardial ischemia/reperfusion injury in adult rats. Vitro Cell Dev Biol Anim. 2016;52(3):305–13.
39. Polosukhina D, Singaravelu K, Padanilam BJ. Activation of protein kinase C isozymes protects LLCPK1 cells from H2O2 induced necrotic cell death. Am J Nephrol. 2003;23(6):380–9.
40. Zhang Y, Zhang Y. lncRNA ZFAS1 improves neuronal Injury and inhibits inflammation, oxidative stress, and apoptosis by sponging miR-582 and upregulating NOS3 expression in cerebral Ischemia/Reperfusion Injury. Inflammation. 2020;43(4):1337–50.
41. Xiang X, Zheng L, Li X. Silencing of long noncoding RNA zinc finger antisense 1 protects against Hypoxia/Reoxygenation-induced Injury in HL-1 cells through targeting the miR-761/Cell death inducing p53 target 1 Axis. J Cardiovasc Pharmacol. 2020;76(5):564–73.
42. Huang P, Yang D, Yu L, Shi Y. Downregulation of lncRNA ZFAS1 protects H9c2 cardiomyocytes from ischemia/reperfusioninduced apoptosis via the miR5903p/NFkappaB signaling pathway. Mol Med Rep. 2020;22(3):2300–6.
43. Zhang Y, Jiao L, Sun L, Li Y, Gao Y, Xu C, et al. LncRNA ZFAS1 as a SERCA2a inhibitor to cause intracellular ca(2+) overload and contractile dysfunction in a mouse model of myocardial infarction. Circ Res. 2018;122(10):1354–68.
44. Lu S, Han L, Hu X, Sun T, Xu D, Li Y, et al. N6-methyladenosine reader IMP2 stabilizes the ZFAS1/OLA1 axis and activates the Warburg effect: implication in colorectal cancer. J Hematol Oncol. 2021;14(1):188.
45. Han CG, Huang Y, Qin L. Long non-coding RNA ZFAS1 as a novel potential biomarker for Predicting the prognosis of thyroid Cancer. Med Sci Monit. 2019;25:2984–92.